ATLAS NOTE

ATLAS-CONF-2012-093

July 5, 2012

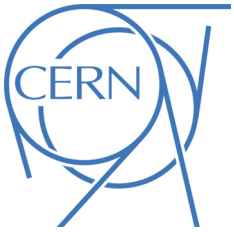

Observation of an Excess of Events in the Search for the Standard Model Higgs boson with the ATLAS detector at the LHC

The ATLAS Collaboration

Abstract

A preliminary combined search for the Standard Model Higgs boson with the ATLAS detector at the LHC is presented. The pp collisions datasets used correspond to integrated luminosities of 4.6 fb^{-1} to 4.9 fb^{-1} at $\sqrt{s}$ = 7 TeV in 2011 and 5.8 fb^{-1} to 5.9 fb^{-1} at $\sqrt{s}$ = 8 TeV in 2012. Searches for $H \to \gamma\gamma$, $H \to ZZ^{(*)}$, $H \to WW^{(*)}$, $H \to b\bar{b}$, and $H \to \tau^+\tau^-$ have been performed on the 2011 data, while only the $H \to \gamma\gamma$ and $H \to ZZ^{(*)} \to \ell^+\ell^-\ell^+\ell^-$ searches are improved compared to previous analyses and use both the 2011 and 2012 data. The Standard Model Higgs boson is excluded at the 95% confidence level for masses in the range 110 GeV to 122.6 GeV and 129.7 GeV to 558 GeV. An excess of events is observed for a Higgs boson mass hypothesis near 126.5 GeV. The local significance of this excess is 5.0σ, where the expected significance in the presence of a Standard Model Higgs boson for that mass hypothesis is 4.6σ.

© Copyright 2012 CERN for the benefit of the ATLAS Collaboration.
Reproduction of this article or parts of it is allowed as specified in the CC-BY-3.0 license.

ATLAS-CONF-2012-093
09 July 2012

1 Introduction

Based on pp collision data taken in 2011 at $\sqrt{s}$ = 7 TeV, the ATLAS Collaboration reported an indication of an excess for Standard Model (SM) Higgs boson with a mass near ~126.5 GeV with a local significance of 2.9 standard deviations (σ) [1]. The global probability for the background to produce an excess at least as significant anywhere in the entire explored Higgs boson mass range of 110–600 GeV was estimated to be ~15%. The mass ranges from 110.0 GeV to 117.5 GeV, 118.5 GeV to 122.5 GeV, and 129 GeV to 539 GeV were excluded at 95% confidence level (CL). The CMS collaboration performed a similar analysis of data collected in 2011, and found an excess corresponding to a local significance of 2.8 σ for $m_H \sim 125$ GeV [2]. The CDF and D0 collaborations at the Tevatron have also reported an excess in the low mass region, in their combined searches for the SM Higgs boson in $p\overline{p}$ collisions [3]. The combined LEP limit [4] excludes a SM Higgs boson with a mass below 114.4 GeV at 95% CL.

These results have made the remaining mass region around 125 GeV the primary focus of the Higgs searches. This note describes the preliminary results from an improved analysis of the 2011 data and the additional 2012 data collected at $\sqrt{s}$ = 8 TeV.

In the Standard Model [5–7], electroweak symmetry breaking is achieved via the Higgs mechanism, which results in a new particle referred to as the Higgs boson [8–13]. The Higgs boson mass, m_H, is a free parameter of the SM. However, for a given m_H hypothesis, the production cross sections and branching ratios can be predicted. Searches for the Higgs boson in ATLAS are currently performed for twelve Higgs boson decay modes, taking into account subsequent decays of vector bosons and tau leptons. These channels are further subdivided according to lepton flavor, the presence of additional jet activity, kinematic regions, and other experimental factors in order to enhance the sensitivity. An overview of the channels is given in Table 1.

By July 2012, the LHC delivered to ATLAS 6.6 fb^{-1} of pp collisions at a center-of-mass energy of 8 TeV of which 6.2 fb^{-1} were collected. In general, the increase in center-of-mass energy, with respect to the 7 TeV data taken in 2011, increases the signal production cross sections more than those of the backgrounds in all channels. The resulting increase in sensitivity of the analyses due to the increase in energy is equivalent to an increase in integrated luminosity of approximately 15–20%. During 2012, the instantaneous luminosity reached record levels of approximately $7 \cdot 10^{33}$ cm^{-2}s^{-1}, almost double the peak luminosity of 2011 with the same 50 ns bunch spacing. The increased luminosity thus came at the expense of an unprecedented number of pp collisions per bunch crossing (pile-up), where the peak number of collisions corresponded to about 30 on average.

Due to the challenging running conditions of 2012, only the $H \to \gamma\gamma$ and $H \to ZZ^{(*)} \to \ell^+\ell^-\ell^+\ell^-$ channels, the two analyses most robust against pile-up, have been updated so far. The analysis of the 2011 data in these two channels has also been updated to benefit from improvements that have been made since the published result, which enhance the sensitivity to the SM Higgs boson. For m_H=126.5 GeV the expected significance in the presence of a SM from these two channels combined improves by ~ 25% with respect to the results presented in Ref. [1]. All the other channels are unchanged with respect to Ref. [1].

2 Additions and Updates to 2011 Combination

2.1 $H \to \gamma\gamma$

The $H \to \gamma\gamma$ search is carried out for m_H hypotheses between 110 GeV and 150 GeV. The datasets used correspond to an integrated luminosity of 4.9 fb^{-1} of pp collisions collected at $\sqrt{s}$ = 7 TeV in 2011 and 5.9 fb^{-1}of pp collisions taken at $\sqrt{s}$ = 8 TeV in 2012 [14]. For this improved 2011 data analysis, the photon identification has been updated to use a neural network algorithm combining variables related

Table 1: Summary of the individual channels entering the combination. The transition points between separately optimized m_H regions are indicated when applicable. The symbols $\otimes$ and $\oplus$ represent direct products or sums over sets of selection requirements.

Higgs Decay	Subsequent Decay	Sub-Channels	m_H Range [GeV]	$\int \mathrm{L}\, dt$ [fb^{-1}]	Ref.
2011 $\sqrt{s}$ =7 TeV					
$H \to \gamma\gamma$	–	9 sub-channels $\{p_{\mathrm{T}_t} \otimes \eta_\gamma \otimes \text{conversion}\} \oplus \{\text{2-jets}\}$	110–150	4.8	[14]
$H \to ZZ^{(*)}$	$\ell\ell\ell'\ell'$	$\{4e, 2e2\mu, 2\mu2e, 4\mu\}$	110–600	4.8	[15]
	$\ell\ell\nu\bar{\nu}$	$\{ee, \mu\mu\} \otimes \{\text{low, high pile-up}\}$	200–280–600	4.7	[16]
	$\ell\ell q\bar{q}$	$\{b\text{-tagged, untagged}\}$	200–300–600	4.7	[17]
$H \to WW^{(*)}$	$\ell\nu\ell\nu$	$\{ee, e\mu, \mu\mu\} \otimes \{\text{0-jets, 1-jet, 2-jets}\} \otimes \{\text{low, high pile-up}\}$	110–200–300–600	4.7	[18]
	$\ell\nu q\overline{q}'$	$\{e, \mu\} \otimes \{\text{0-jets, 1-jet, 2-jets}\}$	300–600	4.7	[19]
$H \to \tau^+\tau^-$	$\tau_{\text{lep}}\tau_{\text{lep}}$	$\{e\mu\} \otimes \{\text{0-jets}\} \oplus \{\ell\ell\} \otimes \{\text{1-jet, 2-jets, } VH\}$	110–150	4.7	[20]
	$\tau_{\text{lep}}\tau_{\text{had}}$	$\{e, \mu\} \otimes \{\text{0-jets}\} \otimes \{E_{\mathrm{T}}^{\text{miss}} < 20 \text{ GeV}, E_{\mathrm{T}}^{\text{miss}} \geq 20 \text{ GeV}\}$ $\oplus \{e, \mu\} \otimes \{\text{1-jet}\} \oplus \{\ell\} \otimes \{\text{2-jets}\}$	110–150	4.7	
	$\tau_{\text{had}}\tau_{\text{had}}$	$\{\text{1-jet}\}$	110–150	4.7	
$VH \to b\bar{b}$	$Z \to \nu\bar{\nu}$	$E_{\mathrm{T}}^{\text{miss}} \in \{120-160, 160-200, \geq 200 \text{ GeV}\}$	110-130	4.6	[21]
	$W \to \ell\nu$	$p_{\mathrm{T}}^{W} \in \{< 50, 50-100, 100-200, \geq 200 \text{ GeV}\}$	110-130	4.7	
	$Z \to \ell\ell$	$p_{\mathrm{T}}^{Z} \in \{< 50, 50-100, 100-200, \geq 200 \text{ GeV}\}$	110-130	4.7	
2012 $\sqrt{s}$ =8 TeV					
$H \to \gamma\gamma$	–	9 sub-channels $\{p_{\mathrm{T}_t} \otimes \eta_\gamma \otimes \text{conversion}\} \oplus \{\text{2-jets}\}$	110–150	5.9	[14]
$H \to ZZ^{(*)}$	$\ell\ell\ell'\ell'$	$\{4e, 2e2\mu, 2\mu2e, 4\mu\}$	110–600	5.8	[15]

to the shape of the shower in the electromagnetic calorimeter. For the 2012 data analysis, a cut-based identification algorithm is used. The analysis in this channel separates events into ten independent categories of varying sensitivity. Similarly to the analysis of Ref. [22], the categorization is based on the pseudorapidity of each photon, whether it was reconstructed as a converted or unconverted photon, and the momentum component of the diphoton system transverse to the diphoton thrust axis (p_{T_t}).

An additional two-jets category, specifically aimed at selecting events produced in the vector boson fusion (VBF) process, has been added to the analysis for both 2011 and 2012. In this category, events are required to have at least two hadronic jets with pseudorapidities $|\eta_{\text{jet}}| < 4.5$ and transverse momenta in excess of 25 GeV. For the 2012 data sample, the minimum p_{T}^{jet} requirement is raised to 30 GeV for forward jets ($2.5 < |\eta_{\text{jet}}| < 4.5$). The two jets are further required to have a large difference in pseudorapidity ($|\Delta\eta_{jj}| > 2.8$) and a large reconstructed invariant mass ($m_{jj} > 400$ GeV). Jets in the acceptance of the inner tracking system are required to have more than 75% of their associated track momentum matched to the primary vertex. The azimuthal angle difference between the dijet and the diphoton systems is required to be larger than 2.6.

For all categories the diphoton invariant mass distribution is fitted to estimate the background and used as a discriminating variable to distinguish signal and background. The mass resolution is approximately 1.7 GeV for $m_H \sim 126.5$ GeV, varying slightly by category. A detailed description of the $H \to \gamma\gamma$ analysis updates is reported in Ref. [14].

2.2 $H \to ZZ^{(*)} \to \ell^+\ell^-\ell^+\ell^-$

The $H \to ZZ^{(*)} \to \ell^+\ell^-\ell^+\ell^-$ search is performed for m_H hypotheses in the mass range between 110 GeV to 600 GeV. The datasets correspond to an integrated luminosities of 4.8 fb^{-1} and 5.8 fb^{-1}of pp for 2011 and 2012, respectively [15]. The main irreducible $ZZ^{(*)}$ background is estimated using a Monte Carlo simulation. The reducible Z+jets background, which has an impact mostly for low four-lepton invariant masses, is estimated from control regions in the data obtained by loosening the isolation and

impact parameter requirements placed on the sub-leading pair of leptons. The top-quark ($t\bar{t}$) background normalization is simultaneously derived in this control region, and is validated in a separate top-enriched control region in which Z candidates are excluded. The events are categorized according to the lepton flavor combinations. The electron identification criteria have been reoptimized and the muon selection has been complemented with muons reconstructed exclusively in the muon system and muons reconstructed from tracks in the inner detector associated with energy deposits in the calorimeter compatible with minimum ionizing particles. The invariant mass of the lepton pair which is closest in mass to the Z-boson mass is required to be between 50 GeV–106 GeV. The invariant mass of the other lepton pair is required to be smaller than 115 GeV and larger than a threshold ranging from 17.5 GeV to 50 GeV, depending on the reconstructed invariant four-leptons mass. A J/ψ veto is applied on events with same flavor and opposite sign leptons with invariant mass smaller than 5 GeV. Several criteria have been reoptimized, including the transverse momentum of the three leading leptons, the impact parameter significance of all leptons, the calorimeter and track isolation, and the angular separation between the leptons. In addition, a kinematic fit, taking into account the natural width of the Z boson and the energy and momentum resolution, improves the reconstructed Higgs boson mass resolution by ~10%. For $m_{4l} < 190$ GeV, the Z boson mass constraint is only used for the di-lepton pair with highest invariant mass, as one pair must originate from an off-shell Z boson. Each of the four combinations of lepton flavor are treated as independent sub-channels. The mass resolutions are approximately 1.5% in the four-muon channel and 2% in the four-electron channel for m_H~120 GeV. The four-lepton invariant mass is used as a discriminating variable. A detailed description of the analysis updates in this channel is given in Ref. [15].

2.3 Systematic Uncertainties

Systematic uncertainties and the treatment of their correlations are unchanged with respect to Ref. [1] for all channels other than $H \to \gamma\gamma$ and $H \to ZZ^{(*)} \to \ell^+\ell^-\ell^+\ell^-$. The systematic uncertainties in the $H \to \gamma\gamma$ and $H \to ZZ^{(*)} \to \ell^+\ell^-\ell^+\ell^-$ channels have been estimated for both the 2011 and 2012 LHC running conditions. The treatment of systematic uncertainties associated with electron and photon energy scales has been updated to a more detailed model improving the treatment of correlations between electrons, converted photons, and unconverted photons.

Individual sources of systematic uncertainty affecting both 2011 and 2012 data are taken as fully correlated. The ±3.9% uncertainty on the measurement of the integrated luminosity for 2011 data is considered uncorrelated with the ±3.6% uncertainty on the measurement of the integrated luminosity in the 2012 data. Furthermore, the $H \to \gamma\gamma$ and $H \to ZZ^{(*)} \to \ell^+\ell^-\ell^+\ell^-$ analyses now use an updated measurement of the integrated luminosity in 2011, which is 1.5% lower than the previous measurement with an improved uncertainty of ±1.8% [**?**]. Since the leading uncertainties in the two estimates of the 2011 integrated luminosity arise from different sources the two estimates are treated as uncorrelated. A detailed review of all systematic uncertainties in the $H \to \gamma\gamma$ and $H \to ZZ^{(*)} \to \ell^+\ell^-\ell^+\ell^-$ analyses is given in Refs. [14, 15].

3 Results

For each Higgs boson mass hypothesis the parameter of interest is the overall signal strength factor μ, which acts as a scale factor to the total rate of signal events. This global factor is used for all pairings of production cross sections and branching ratios. The signal strength is defined such that $\mu = 0$ corresponds to the background-only model and $\mu = 1$ corresponds to the SM Higgs boson signal. The combination procedure used herein and described in Refs. [1, 23–25] is based on the profile likelihood ratio test statistic $\lambda(\mu)$ [26]. The test statistic extracts the information on the signal strength from the full likelihood including all the parameters describing the systematic uncertainties and their correlations, and is designed

to be powerful in the presence of a SM Higgs. Exclusion limits are based on the CL_s prescription [27]; a value of μ is regarded as excluded at the 95% CL when CL_s is less than 5%. The statistical procedures are performed in a scan over the hypothesized value of the Higgs boson mass, and m_H is held fixed in the likelihood function.

The combined 95% CL exclusion limits on μ are shown in Fig. 1 as a function of m_H. These results are based on the asymptotic approximation [26]. This procedure has been validated using ensemble tests and a Bayesian calculation of the exclusion limits with a uniform prior on the signal cross section. Typically, these two alternative approaches agree with the expected results from asymptotic approximations to within a few percent.

The expected 95% CL exclusion region covers the m_H range from 110 GeV to 582 GeV. The observed 95% CL exclusion regions are from 110 GeV to 122.6 GeV and 129.7 GeV to 558 GeV. The addition of the 2012 $H \to \gamma\gamma$ and $H \to ZZ^{(*)} \to \ell^+\ell^-\ell^+\ell^-$ analyses as well as the improvements to the analysis of 2011 data in these two channels bring a significant gain in sensitivity in the low-mass region with respect to the previous combined search [1]. Figure 2 shows the CL_s values for $\mu = 1$, where it can be seen that the regions between 111.7 GeV to 121.8 GeV and 130.7 GeV to 523 GeV are excluded at the 99% CL. The observed exclusion covers a large part of the expected exclusion range (113.0 GeV to 522 GeV), with the exception of the low mass region between 121.8 GeV and 130.7 GeV.

An excess of events is observed near m_H~126.5 GeV in the $H \to \gamma\gamma$ and $H \to ZZ^{(*)} \to \ell^+\ell^-\ell^+\ell^-$ channels, both of which provide fully reconstructed candidates with high resolution in invariant mass. The significance of an excess is quantified by the probability (p_0) that a background-only experiment is more signal-like than that observed. The local p_0 probability is assessed for a fixed m_H hypothesis and the equivalent formulation in terms of number of standard deviations is referred to as the local significance. The probability for a background-only experiment to produce a local significance of this size or larger anywhere in a given mass region is referred to as the global p_0. The corresponding reduction in the significance is referred to as the "trials factor" or "look-elsewhere effect" and is estimated using the prescription described in Refs. [24, 28].

The observed local p_0 values calculated using the asymptotic approximation as a function of m_H are shown in Fig. 3. The expected p_0 corresponds to the median p_0 in the presence of a SM Higgs boson signal at that mass. The corresponding significances are shown in Fig. 4. In order to validate the asymptotic approximation for such extremely small p-values, an importance sampling algorithm has been used.

The largest local significance for the combined 2011+2012 analysis is found for a SM Higgs boson mass hypothesis of m_H=126.5 GeV, where it reaches 5.1σ, with an expected value in the presence of a SM Higgs boson signal at that mass of 4.6σ. For the 2012 data alone, the maximum local significance for the $H \to \gamma\gamma$ and $H \to ZZ^{(*)} \to \ell^+\ell^-\ell^+\ell^-$ channels combined is 4.0σ, which occurs at $m_H = 127.0$ GeV (3.4σ expected).

The significance of the excess is mildly sensitive to energy scale systematic (ESS) uncertainties and resolution for photons and electrons. The muon energy scale systematic uncertainties are smaller and therefore neglected. The presence of these uncertainties, which affect the shape and position of the signal distributions, lead to a small deviation in the distribution of the test statistic from a chi-square distribution. Previously, the observed p_0 including these effects was estimated using ensemble tests; however, the very small p_0 values makes this impractical computationally.

Here, a new approach to correcting for the leading departure from the asymptotic chi-square distribution is employed. The procedure is motivated by the observation that in the limit of very large energy scale uncertainties, an invariant mass peak could occur almost anywhere with m_H fixed. This is essentially equivalent to the situation where m_H is allowed to float freely in the fit, which gives rise to the look-elsewhere effect. The procedure outlined in Ref. [24, 28], which follows from theoretical work in

Ref. [29], corrects the minimum local p-value to the global p-value via

$$p_0^{\text{global}} = p_0^{\text{min local}} + Ne^{-(q_0(m_H)-u)/2} , \quad (1)$$

where N is the average number of times the test statistic $q_0(m_H)$ crosses some fixed value u while scanning m_H in the range considered. This corresponds to replacing the fixed threshold u in the equation above with $u(m_H)$, a parabolic form related to the assumed Gaussian distribution of the energy scale uncertainty. A generalization of the fixed u result [30] can be used to find the expected number of times the test statistic $q_0(m_H)$ is greater than $u(m_H)$. In essence, the correction to the local p-value due to energy scale systematics is similar to a look-elsewhere effect correction in a small search range. The effective size of the range, however, depends on the details of how several components to the energy scale uncertainty affect the ten different $H \to \gamma\gamma$ channels and four $H \to ZZ^{(*)} \to \ell^+\ell^-\ell^+\ell^-$ channels. The effective N can be estimated by fitting the sum of a chi-square and a falling exponential to the distribution of the test statistic created with a large number of pseudo-experiments. This hybrid ensemble-asymptotic approach was validated with much larger samples of pseudo-experiments generated for the previous combination [1] and shown to accurately reproduce the p-values. The result of this procedure for the full combined 2011+2012 model results in a local significance including energy scale systematics of 5.0σ.

The global significance for local excesses depends on the range of m_H and the channels considered. The global significance for the combined search to have a 5.0σ excess anywhere in the mass range 110–600 GeV is estimated to be approximately 4.1σ, increasing to 4.3σ in the range 110–150 GeV which is the range of the $H \to \gamma\gamma$ search and approximately the mass range not excluded at the 99% CL by the LHC combined SM Higgs boson search [31] and the LEP electroweak limits on a Standard Model Higgs boson [4]. The global significance for the 4.0σ excess in the 2012 combined search to occur in the range 110–130.7 GeV, which is not excluded by the 2011 combination at 99% confidence level, is approximately 3.1σ.

The best-fit value of μ, denoted $\hat{\mu}$, is displayed for the combination of all channels in Fig. 5 as a function of the m_H hypothesis. The bands around $\hat{\mu}$ illustrate the μ interval corresponding to $-2\ln\lambda(\mu) < 1$ and represent an approximate $\pm 1\sigma$ variation. While the estimator $\hat{\mu}$ is allowed to be negative in Fig. 5 in order to illustrate the presence and extent of downward fluctuations, the μ parameter is bounded to ensure non-negative values of the probability density functions in the individual channels. Hence, for negative $\hat{\mu}$ values close to the boundary, the $-2\ln\lambda(\mu) < 1$ region does not reflect a calibrated 68% confidence interval. It should be noted that $\hat{\mu}$ does not directly provide information on the relative strength of the production modes, nor does its maximum value give an estimate of the mass of a potential signal.

The best fit values of the signal strength parameter for each channel independently and for the combination are illustrated in Fig. 7 for $m_H = 126.5$ GeV . The observed excess corresponds to $\hat{\mu}$ of approximately 1.2 ± 0.3 for $m_H = 126.5$ GeV with all 2011 and 2012 channels combined. This signal strength is consistent with the SM Higgs boson hypothesis $\mu = 1$.

Neither the m_H value that minimizes p_0 nor the one that maximizes $\hat{\mu}$ are unbiased estimates of the SM Higgs boson mass m_H as they are computed using a fixed m_H hypothesis. The maximum likelihood estimate of m_H from the combined likelihood remains subject to further studies; however, likelihood contours of (μ, m_H) in the $H \to \gamma\gamma$ and $H \to ZZ^{(*)} \to \ell^+\ell^-\ell^+\ell^-$ channels are presented in Appendix A. The probability for a single Higgs boson-like resonance to produce mass peaks separated by larger than the amount observed in these two channels, allowing the signal strengths to vary independently, is about 20%.

4 Conclusion

Searches for the SM Higgs boson have been performed in the $H \to \gamma\gamma$ and $H \to ZZ^{(*)} \to \ell^+\ell^-\ell^+\ell^-$ channels with the ATLAS experiment at the LHC using 5.8–5.9 fb^{-1}of pp collisions collected at a center-

of-mass energy of 8 TeV. These 2012 results are combined with the earlier 2011 results [1] based on an integrated luminosity of 4.7–4.9 fb^{-1}, including improved $H \to \gamma\gamma$ and $H \to ZZ^{(*)} \to \ell^+\ell^-\ell^+\ell^-$ analyses.

The observed SM Higgs boson exclusion ranges at the 95% CL are 110 GeV to 122.6 GeV and 129.7 GeV to 558 GeV, while masses between 110 GeV to 582 GeV are expected to be excluded at the 95% CL.

A significant 5σ excess of events is observed in the search for the Standard Model Higgs boson, dominated by the two channels with the highest mass resolutions. This observation provides evidence for a new, narrow resonance at a mass near 126.5 GeV. Although the combined result including all search channels is consistent with the production and decay of a Standard Model Higgs boson, more data are needed to assess the nature of this excess.

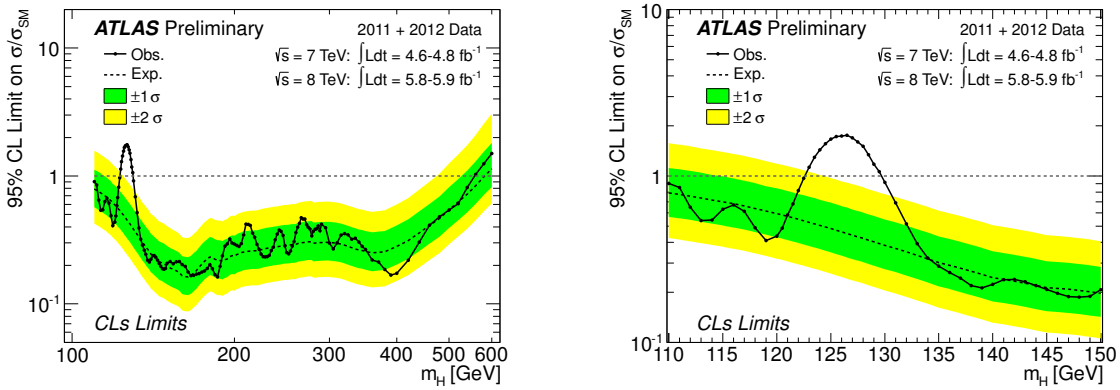

Figure 1: The observed (full line) and expected (dashed line) 95% CL combined upper limits on the SM Higgs boson production cross section divided by the Standard Model expectation as a function of m_H in the full mass range considered in this analysis (a) and in the low mass range (b). The dashed curves show the median expected limit in the absence of a signal and the green and yellow bands indicate the corresponding 68% and 95% intervals.

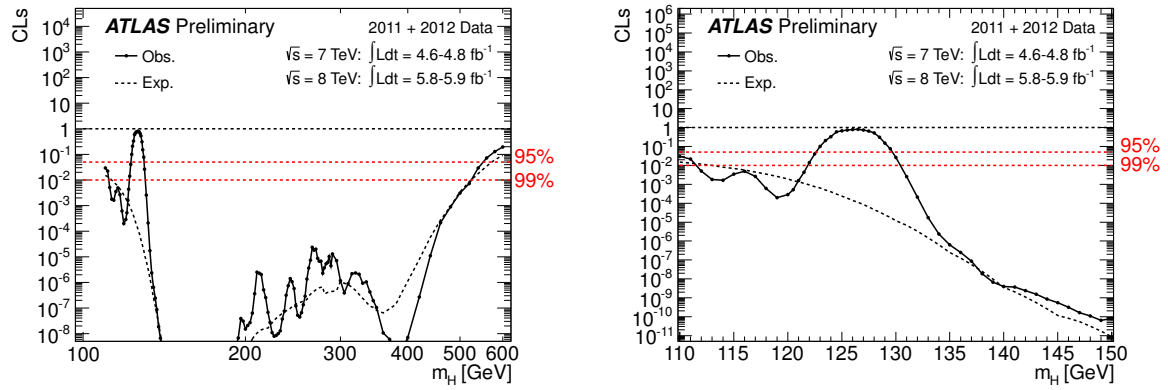

(a) (b)

Figure 2: The value of the combined CL_s for $\mu = 1$ (testing the Standard Model Higgs boson hypothesis) as a function of m_H in the full mass range of this analysis (a) and in the low mass range (b). The expected CL_s is shown in the dashed curves. The regions with $CL_s < \alpha$ are excluded at least at $(1 - \alpha)$ CL. The 95% and 99% CL values are indicated as dashed horizontal lines.

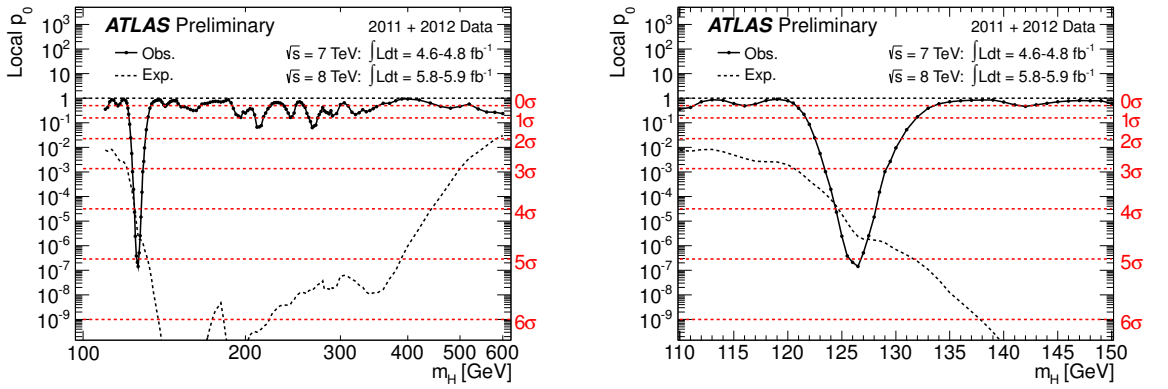

(a) (b)

Figure 3: The local probability p_0 for a background-only experiment to be more signal-like than the observation in the full mass range of this analysis (a) and in the low mass range (b) as a function of m_H. The dashed curves show the median expected local p_0 under the hypothesis of a Standard Model Higgs boson production signal at that mass. The horizontal dashed lines indicate the p-values corresponding to significances of 1σ to 6σ. Energy scale systematics are not included; taking them into account leads to a small negative correction $\sim 0.1\sigma$ near m_H=126 GeV.

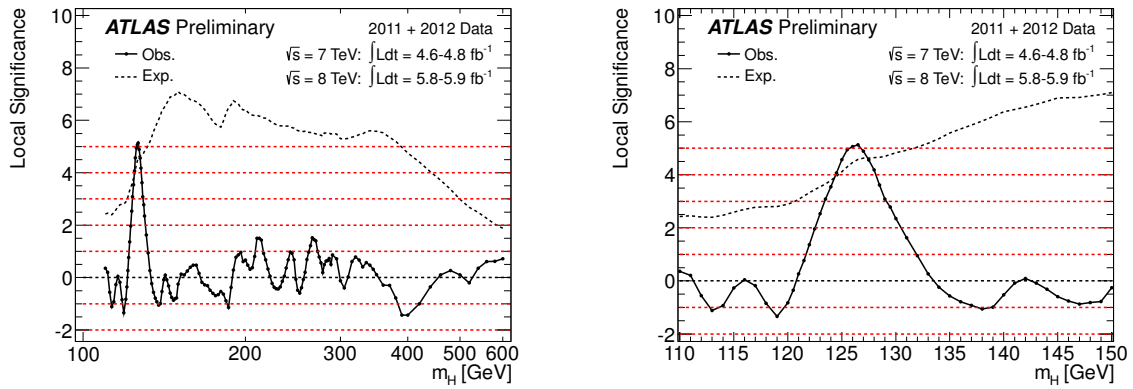

(a) (b)

Figure 4: The same as Fig. 3 shown in terms of local significance. An excess (deficit) of events corresponds to a positive (negative) local significance. This presentation makes clear the magnitude of a local deficit of events, where the logarithmic scale in Fig. 3 compresses large values of p_0. The dashed curves show the median expected local p_0 under the hypothesis of a Standard Model Higgs boson production signal at that mass. The horizontal dashed lines indicate significances ranging from -2σ to 5σ. Energy scale systematics are not included; taking them into account leads to a small correction $\sim$ 0.1σ near m_H=126 GeV.

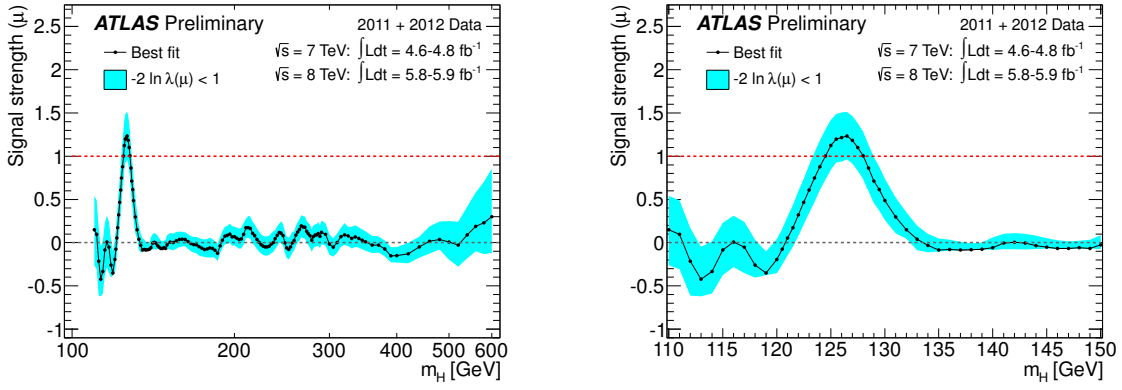

(a) (b)

Figure 5: The combined best-fit signal strength $\hat{\mu}$ as a function of the Higgs boson mass hypothesis (a) in the full mass range of this analysis and (b) in the low mass range. The interval around $\hat{\mu}$ corresponds to a variation of $-2\ln\lambda(\mu) < 1$.

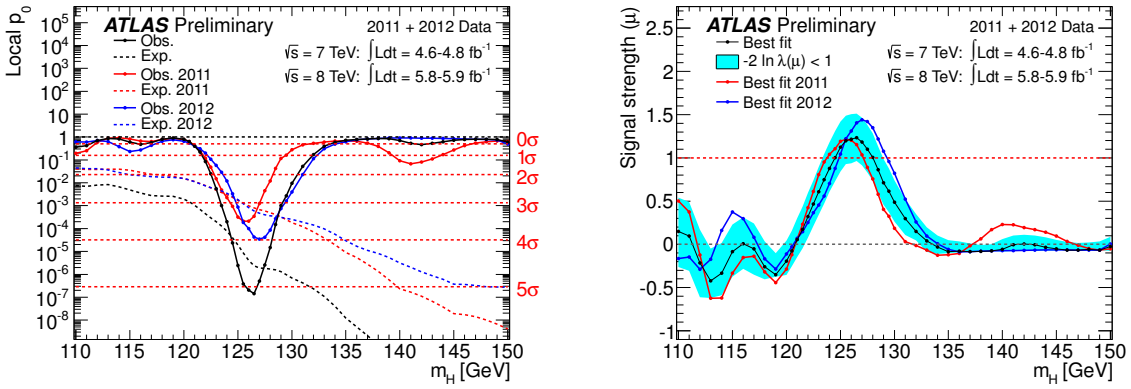

(a) (b)

Figure 6: The evolution of the local probability p_0 and the best-fit signal strength $\hat{\mu}$ from the 2011 data, the 2012 data, and their combination.

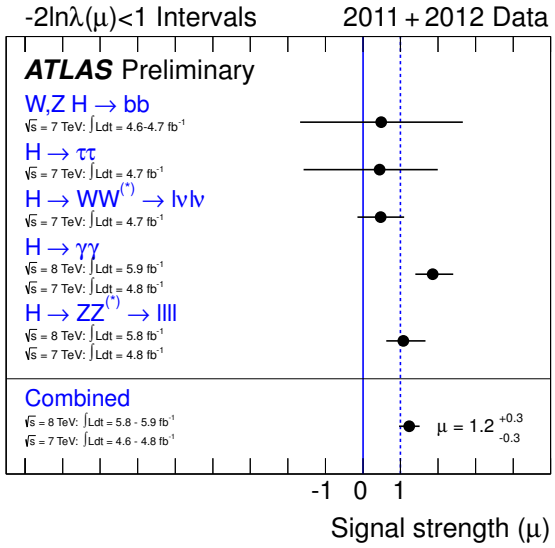

Figure 7: Summary of the individual and combined best-fit values of the strength parameter for a Higgs boson mass hypothesis of 126.5 GeV.

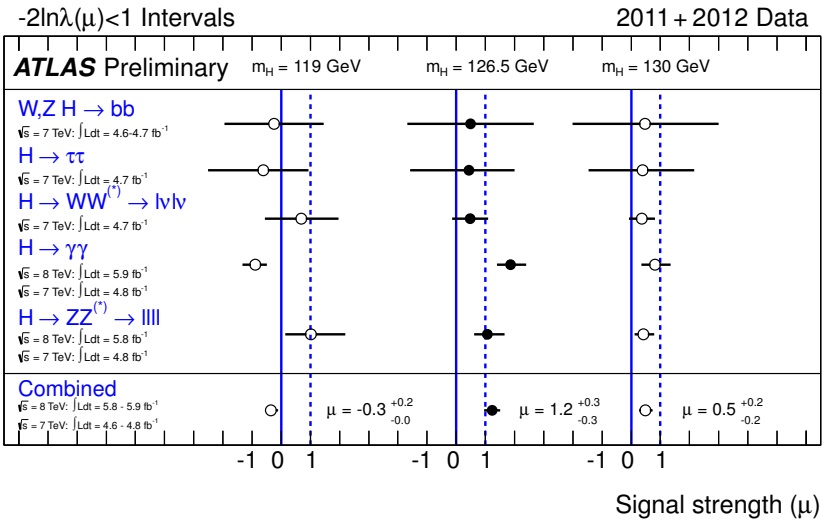

Figure 8: Summary of the individual and combined best-fit values of the strength parameter for three sample Higgs boson mass hypotheses of 119 GeV, 126.5 GeV and 130 GeV.

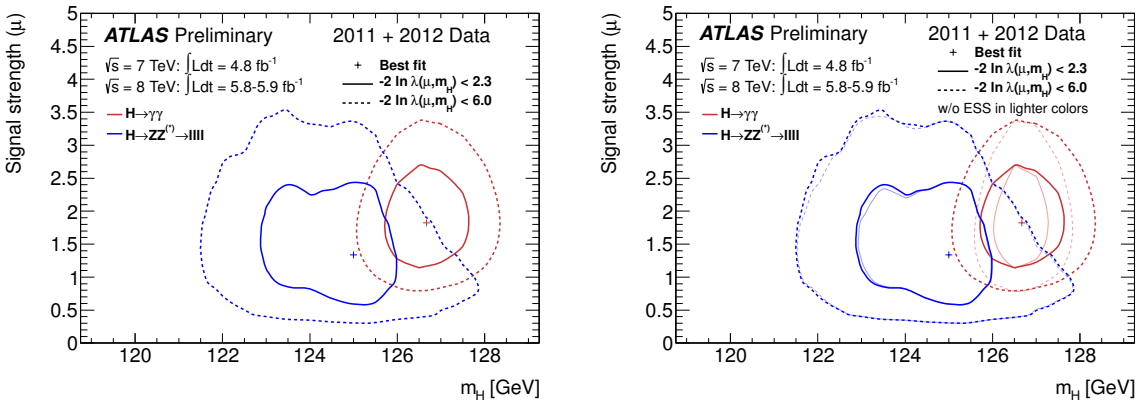

(a) (b)

Figure 9: Likelihood contours in (μ, m_H) for the $H \to ZZ^{(*)} \to \ell^+\ell^-\ell^+\ell^-$ and $H \to \gamma\gamma$ channels including energy scale systematics are shown in panel (a). The comparison of the contours with (thick lines) and without (thin lines in lighter colors) energy scale systematics is shown in panel (b).

Appendix A: Contours in (μ, m_H) for $H \to \gamma\gamma$ and $H \to ZZ^{(*)} \to \ell^+\ell^-\ell^+\ell^-$

The results presented so far do not give any information about the range of masses consistent with a potential signal, because the statistical procedure is performed in a scan over m_H with m_H fixed in the likelihood as if it were known a priori. These shortcomings are addressed by considering various contours of the likelihood function.

In order to address the values of the signal strength and mass of a potential signal that are simultaneously consistent with the data, the following profile likelihood ratio is used:

$$\lambda(\mu, m_H) = \frac{L(\mu, m_H, \hat{\hat{\boldsymbol{\theta}}}(\mu, m_H))}{L(\hat{\mu}, \hat{m}_H, \hat{\boldsymbol{\theta}})} \,, \tag{2}$$

were $\hat{\hat{\boldsymbol{\theta}}}(\mu, m_H)$ is the conditional maximum likelihood estimate with μ and m_H fixed. In the presence of a strong signal, this test statistic will produce closed contours about the best fit point $(\hat{\mu}, \hat{m}_h)$; while in the absence of a signal the contours will be upper limits on μ for all values of m_H.

Asymptotically, the test statistic $-2\ln\lambda(\mu, m_H)$ is distributed as a χ^2 distribution with two degrees of freedom. In particular, the $100(1-\alpha)\%$ confidence level contours are defined by $-2\ln\lambda(\mu, m_H) < k_\alpha$, where k_α satisfies $P(\chi^2_2 > k_\alpha) = \alpha$.

The 68% and 95% CL contours for the $H \to \gamma\gamma$ channel are shown in Fig 9, where the asymptotic approximations have been validated with ensembles of pseudo-experiments. Similar contours for the $H \to ZZ^{(*)} \to \ell^+\ell^-\ell^+\ell^-$ channel are shown in Fig 9, where the distribution of $-2\ln\lambda(\mu, m_H)$ is not expected to have converged to the asymptotic distribution. These preliminary contours in the (μ, m_H) plane take into account uncertainty in the energy scale and resolution. The impact of these uncertainties is illustrated in Fig. 9(b).

The probability for a single Higgs boson-like resonance to produce mass peaks separated by larger than the amount observed in these two channels, allowing the signal strengths to vary independently, is about 20%.

Appendix B: Individual Channels and Combined Results

The individual channels observed and expected results in terms of CL limits, local probability p_0 and the corresponding significance are shown in Fig. 10, Fig. 11, and Fig. 12. The expected only results are shown in Fig. 13, Fig. 14, and Fig. 15.

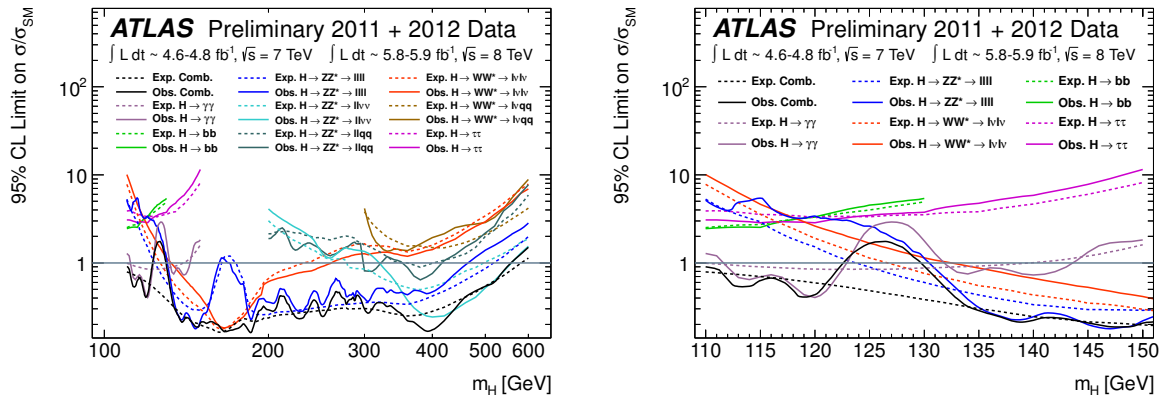

(a) (b)

Figure 10: The observed (solid) and expected (dashed) 95% CL cross section upper limits for the individual search channels and the combination, normalized to the SM Higgs boson production cross section, as a function of the Higgs boson mass hypothesis; (a) for the full Higgs boson mass hypotheses range and (b) in the low mass range. The expected limits are those for the background-only hypothesis i.e. in the absence of a Higgs boson signal.

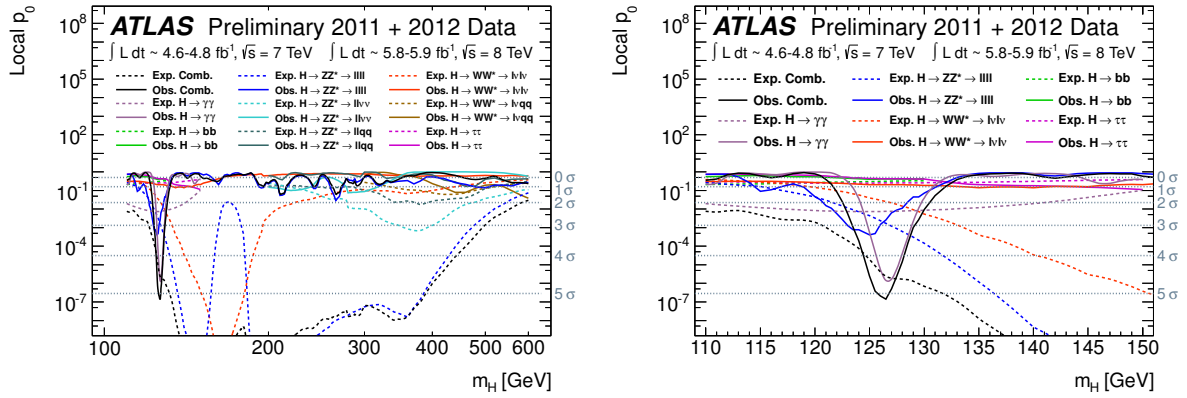

(a) (b)

Figure 11: The local probability p_0 for a background-only experiment to be more signal-like than the observation, for individual channels and the combination; (a) in the full mass range of 110–600 GeV and (b) in the low mass range of 110–150 GeV. The full curves give the observed individual and combined p_0. The dashed curves show the median expected value under the hypothesis of a SM Higgs boson signal at that mass. The horizontal dashed lines indicate the p_0 corresponding to significances of 1σ, 2σ, 3σ, 4σ and 5σ.

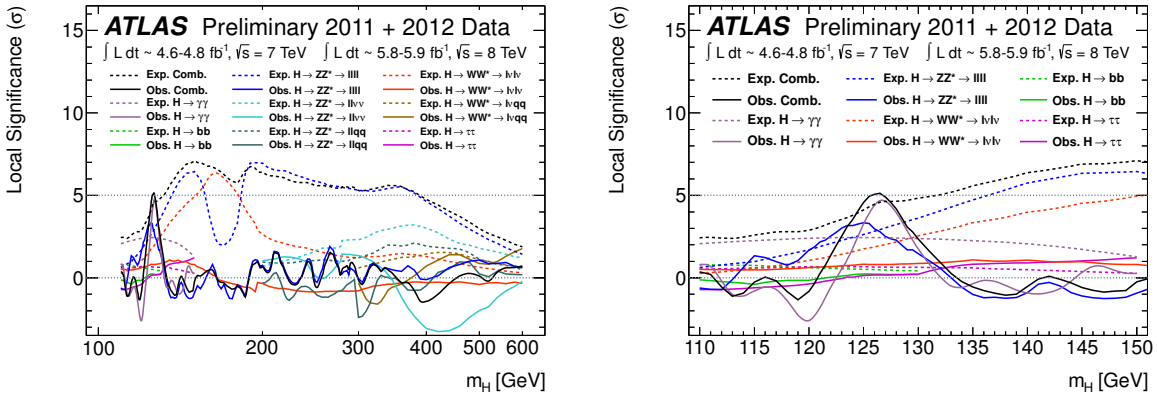

(a) (b)

Figure 12: The local significance in terms of standard deviations for individual channels and the combination; (a) in the full mass range of 110–600 GeV and (b) in the low mass range of 110–150 GeV. The full curves give the observed individual and combined local significances. The dashed curves show the median expected value under the hypothesis of a SM Higgs boson signal at that mass.

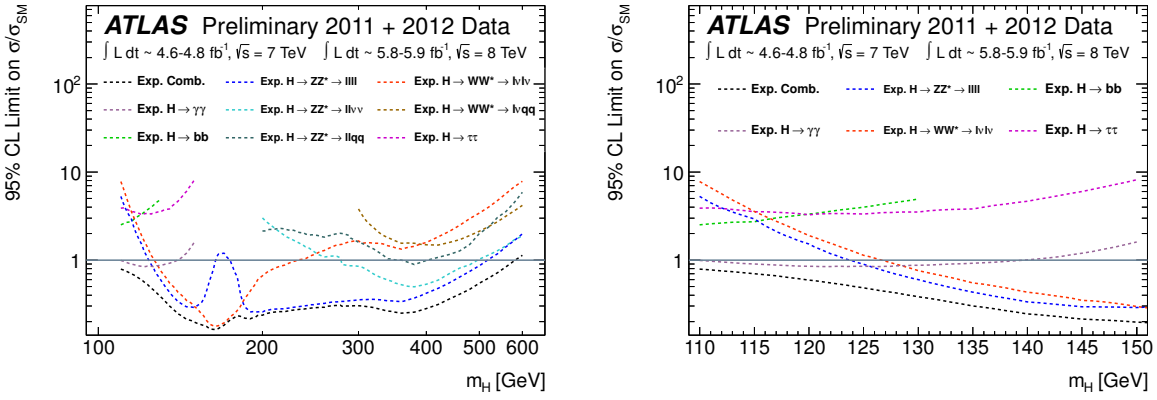

(a) (b)

Figure 13: The expected 95% CL cross section upper limits for the individual search channels and the combination, normalized to the SM Higgs boson production cross section, as a function of the Higgs boson mass hypothesis; (a) for the full Higgs boson mass hypotheses range and (b) in the low mass range. The expected limits are those for the background-only hypothesis i.e. in the absence of a Higgs boson signal.

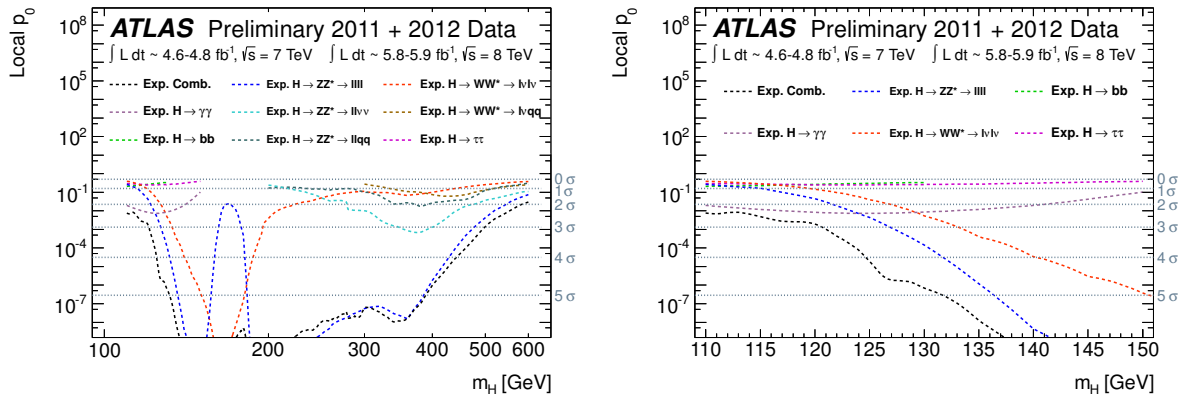

(a) (b)

Figure 14: The expected local probability p_0 for a background-only experiment to be more signal-like than the observation, for individual channels and the combination; (a) in the full mass range of 110–600 GeV and (b) in the low mass range of 110–150 GeV. The horizontal dashed lines indicate the p_0 corresponding to significances of 1σ to 5σ.

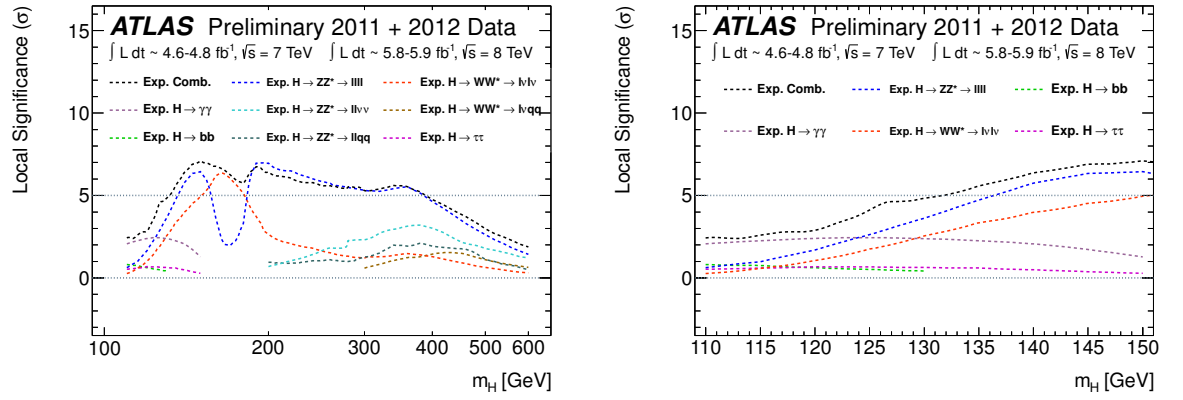

(a) (b)

Figure 15: The expected local significance in terms of standard deviations for individual channels and the combination. (a) In the full mass range of 110–600 GeV and (b) in the low mass range of 110–150 GeV.

Appendix C: Results from 2012

The primary results are shown here for the combination of the 2012 $H \to \gamma\gamma$ and $H \to ZZ^{(*)} \to \ell^+\ell^-\ell^+\ell^-$ search channels alone.

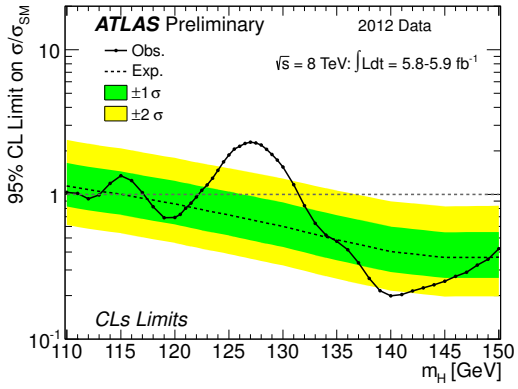

Figure 16: The observed (full line) and expected (dashed line) 95% CL combined upper limits on the SM Higgs boson production cross section divided by the Standard Model expectation as a function of m_H for the $H \to \gamma\gamma$ and $H \to ZZ^{(*)} \to \ell^+\ell^-\ell^+\ell^-$ analysis on 2012 data. The dashed curve shows the median expected limit in the absence of a signal and the green and yellow bands indicate the corresponding 68% and 95% intervals.

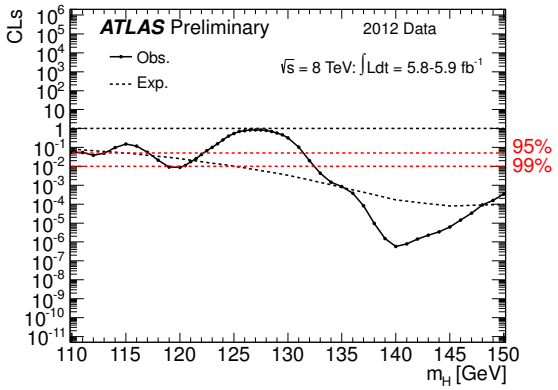

Figure 17: The value of the combined CL_s for $\mu = 1$ (testing the Standard Model Higgs boson hypothesis) as a function of m_H for the $H \to \gamma\gamma$ and $H \to ZZ^{(*)} \to \ell^+\ell^-\ell^+\ell^-$ analysis on 2012 data. The regions with $CL_s < \alpha$ are excluded at least at $(1 - \alpha)$ CL. The 95% and 99% CL values are indicated as dashed lines.

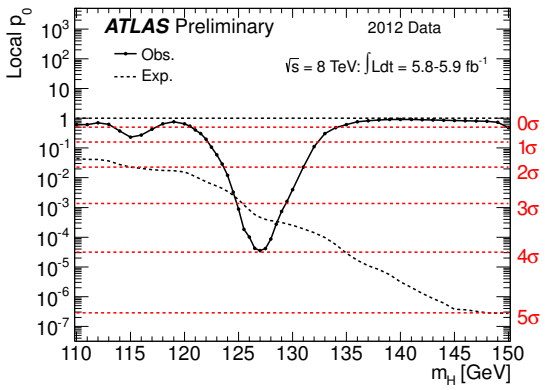

Figure 18: The local probability p_0 for a background-only experiment to be more signal-like than the observation as a function of m_H for the $H \to \gamma\gamma$ and $H \to ZZ^{(*)} \to \ell^+\ell^-\ell^+\ell^-$ analysis on 2012 data. The dashed curves show the median expected local p_0 under the hypothesis of a Standard Model Higgs boson production signal at that mass. The horizontal dashed lines indicate the p-values corresponding to significances of 1σ to 5σ.

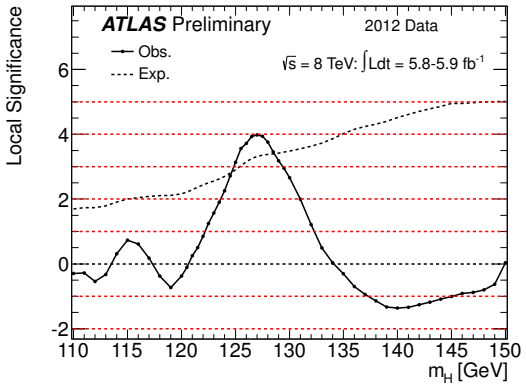

Figure 19: The same as Fig. 18 shown in terms of local significance. An excess (deficit) of events corresponds to a positive (negative) local significance. This presentation makes clear the magnitude of a local deficit of events, where the logarithmic scale in Fig. 18 compresses large values of p_0. The dashed curves show the median expected local p_0 under the hypothesis of a Standard Model Higgs boson production signal at that mass. The horizontal dashed lines indicate significances ranging from -2σ to 5σ. Energy scale systematics are not included.

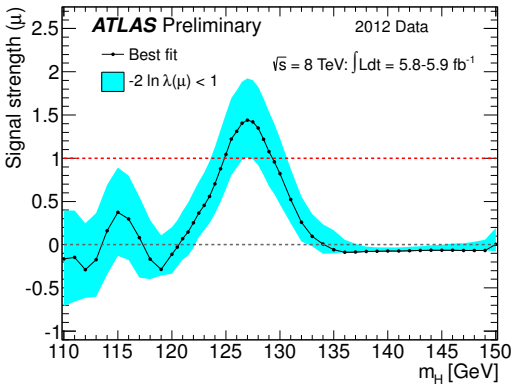

Figure 20: The combined best-fit signal strength $\hat{\mu}$ as a function of the Higgs boson mass hypothesis for the combination of the 2012 $H \to \gamma\gamma$ and $H \to ZZ^{(*)} \to \ell^+\ell^-\ell^+\ell^-$ analysis. The interval around $\hat{\mu}$ corresponds to a variation of $-2\ln\lambda(\mu) < 1$.

Appendix D: Alternative Combinations

In order to compare the results obtained in the high mass resolution channels, $H \to \gamma\gamma$ and $H \to ZZ^{(*)} \to \ell^+\ell^-\ell^+\ell^-$, with those of low mass resolution $H \to WW^{(*)} \to \ell^+\nu\ell^-\overline{\nu}$, $H \to \tau^+\tau^-$ and $H \to b\bar{b}$, a separate combination of these channels is performed. The results are illustrated in Fig. 21.

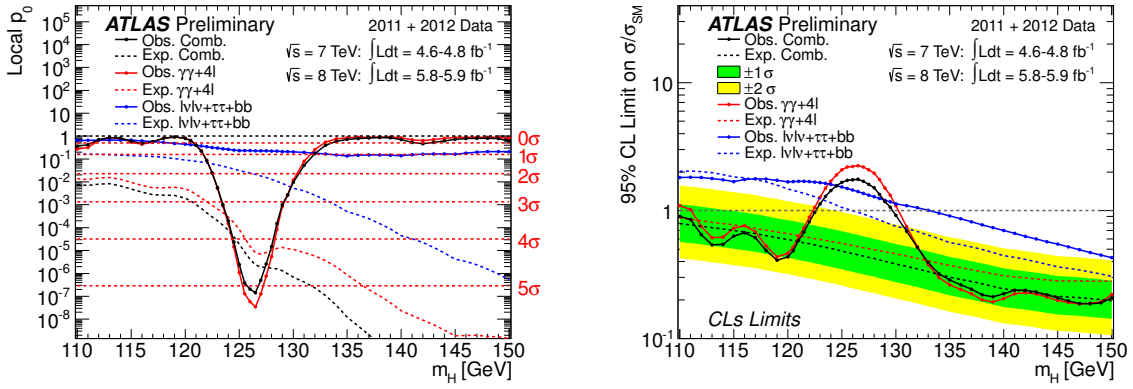

(a) (b)

Figure 21: (a) The local probability p_0 for a background-only experiment to be more signal-like than the observation and (b) the 95% CL upper limit on the Standard Model Higgs boson production cross section divided by the SM expectation as a function of m_H is indicated by the solid curves for the combination of the high mass resolution $H \to \gamma\gamma$ and $H \to ZZ^{(*)} \to \ell^+\ell^-\ell^+\ell^-$ channels (red), the low mass resolution channels $H \to WW^{(*)} \to \ell^+\nu\ell^-\overline{\nu}$, $H \to \tau^+\tau^-$ and $H \to b\bar{b}$ channels (blue), and all channels (black). The dashed curves show (a) the median expected p_0 value under the hypothesis of a SM Higgs boson signal at that mass and (b) the median expected limit in the absence of a signal. The green and yellow bands indicate the corresponding 68% and 95% intervals for the full combination.

References

[1] ATLAS Collaboration, *Combined search for the Standard Model Higgs boson in pp collisions at $\sqrt{s}$ = 7 TeV with the ATLAS detector*, submitted to Phys. Rev. D (2012), arXiv:1207.0319 [hep-ex].

[2] CMS Collaboration, *Combined results of searches for the standard model Higgs boson in pp collisions at $\sqrt{s}$ = 7 TeV*, Phys. Lett. **B 710** (2012) 26–48.

[3] CDF and D0 Collaboration, *Combination of Tevatron searches for the Standard Model Higgs boson in the W+W- decay mode*, Phys. Rev. Lett. **104** (2010) 061802.

[4] ALEPH collaboration, DELPHI collaboration, L3 collaboration, OPAL collaboration and the LEP Working Group for Higgs boson searches, *Search for the standard model Higgs boson at LEP*, Phys. Lett. **B 565** (2003) 61–75.

[5] S. L. Glashow, *Partial symmetries of weak interactions*, Nucl. Phys. **22** (1961) 579–588.

[6] S. Weinberg, *A model of leptons*, Phys. Rev. Lett. **19** (1967) 1264–1266.

[7] A. Salam, *in Elementary Particle Theory, p. 367*. Almqvist and Wiksell, Stockholm, 1968.

[8] F. Englert and R. Brout, *Broken symmetry and the mass of gauge vector mesons*, Phys. Rev. Lett. **13** (1964) 321–323.

[9] P. W. Higgs, *Broken symmetries, massless particles and gauge fields*, Phys. Lett. **12** (1964) 132–133.

[10] P. W. Higgs, *Broken symmetries and the masses of gauge bosons*, Phys. Rev. Lett. **13** (1964) 508–509.

[11] G. Guralnik, C. Hagen, and T. Kibble, *Global conservation laws and massless particles*, Phys. Rev. Lett. **13** (1964) 585–587.

[12] P. W. Higgs, *Spontaneous symmetry breakdown without massless bosons*, Phys. Rev. **145** (1966) 1156–1163.

[13] T. Kibble, *Symmetry breaking in non-Abelian gauge theories*, Phys. Rev. **155** (1967) 1554–1561.

[14] ATLAS Collaboration, *Observation of an excess of events in the search for the Standard Model Higgs boson in the $\gamma\gamma$ channel with the ATLAS detector*, ATLAS-COM-CONF-2012-109 (2012).

[15] ATLAS Collaboration, *Observation of an excess of events in the search for the Standard Model Higgs boson in the $H \to ZZ^{(*)} \to 4l$ channel with the ATLAS detector*, ATLAS-COM-CONF-2012-106 (2012).

[16] ATLAS Collaboration, *Search for a Standard Model Higgs boson in the $H \to ZZ \to llvv$ decay channel using 4.7 fb^{-1} of $\sqrt{s}$ = 7 TeV data with the ATLAS detector*, arXiv:1205.6744 [hep-ex]. submitted to Phys. Lett. B.

[17] ATLAS Collaboration, *Search for a Standard Model Higgs boson in the mass range 200-600 GeV in the $H \to ZZ \to llqq$ decay channel*, arXiv:1206.2443 [hep-ex]. submitted to Phys. Lett. B.

[18] ATLAS Collaboration, *Search for the Standard Model Higgs boson in theH $\to WW^{(*)} \to \ell^+\nu\ell^-\overline{\nu}$ decay mode with 4.7 $fb^{-1}$of ATLAS data at $\sqrt{s}$ = 7 TeV*, arXiv:1206.0756 [hep-ex]. submitted to Phys. Lett. B.

[19] ATLAS Collaboration, *Search for the Higgs boson in the $H \to WW \to l\nu jj$ decay channel at $\sqrt{s}$ = 7 TeV with the ATLAS detector*, submitted to Phys. Lett. B (2012), arXiv:1206.6074 [hep-ex].

[20] ATLAS Collaboration, *Search for the Standard Model Higgs boson in the $H \to \tau^+\tau^-$ decay*, submitted to JHEP (2012), arXiv:1206.5971 [hep-ex].

[21] ATLAS Collaboration, *Search for the Standard Model Higgs boson produced in association with a vector boson and decaying to a b-quark pair with the ATLAS detector at the LHC*, submitted to Phys. Lett. B (2012), arXiv:1207.0210 [hep-ex].

[22] ATLAS Collaboration, *Search for the Standard Model Higgs boson in the diphoton decay channel with 4.9 fb^{-1} of pp collisions at $\sqrt{s}$ =7 TeV with ATLAS*, Phys. Rev. Lett. **108** (2012) 111803, arXiv:1202.1414 [hep-ex].

[23] ATLAS Collaboration, *Limits on the production of the Standard Model Higgs Boson in pp collisions at $\sqrt{s}$ = 7 TeV with the ATLAS detector*, Eur. Phys. J. **C71** (2010) 1728.

[24] ATLAS and CMS Collaborations, *LHC Higgs Combination Working Group Report*, ATL-PHYS-PUB-2011-011, CERN-CMS-NOTE-2011-005 (2011).

[25] L. Moneta, K. Belasco, K. S. Cranmer, S. Kreiss, A. Lazzaro, et al., *The RooStats Project*, PoS **ACAT2010** (2010) 057.

[26] G. Cowan, K. Cranmer, E. Gross and O. Vitells, *Asymptotic formulae for likelihood-based tests of new physics*, Eur. Phys. J. **C71** (2011) 1554.

[27] A. L. Read, *Presentation of search results: The CL(s) technique*, J. Phys. **G28** (2002) 2693–2704.

[28] E. Gross and O. Vitells, *Trial factors for the look elsewhere effect in high energy physics*, Eur. Phys. J. **C70** (2010) 525–530.

[29] R. B. Davies, *Hypothesis testing when a nuisance parameter is present only under the alternative*, Biometrika **74** no. 1, (1987) 33–43.

[30] M. Leadbetter, *On Crossings of Levels and Curves by a Wide Class of Stochastic Processes*, Ann. Math. Statist **37** no. 1, (1965) 260–267.

[31] ATLAS and CMS Collaborations, *Combined Standard Model Higgs boson searches with up to 2.3 fb^{-1} of pp collisions at $\sqrt{s}$=7 TeV at the LHC*, ATLAS-CONF-2011-157, CMS-PAS-HIG-11-023 (2011).